Generation and Characterization of Well-Defined Zn^{2+} Lewis Acid Sites in Ion Exchanged Zeolite BEA

Jochen Penzien,[†] Anuji Abraham,[‡] Jeroen A. van Bokhoven,[‡] Andreas Jentys,[†] Thomas E. Müller,[†] Carsten Sievers,[†] and Johannes A. Lercher*,[†]

Lehrstuhl für Technische Chemie II, Technische Universität München, Lichtenbergstrasse 4, 85747 Garching, Germany, and Federal Institute of Technology (ETH), 8093-CH Zürich, Switzerland

Received: October 31, 2003; In Final Form: January 19, 2004

Bifunctional, Lewis, and Brønsted acidic molecular sieves were prepared by stepwise zinc ion exchange of zeolite BEA. The relation between the location of the Zn^{2+} cations in the zeolite structure and the Lewis acidity of the metal cations was explored. Several techniques were used for the detailed characterization of the material, including IR spectroscopy, with pyridine and acetonitrile as probe molecules, temperature programmed desorption, with ammonia and 2-propylamine as probe molecules, X-ray absorption spectroscopy, and ^{27}Al MAS and MQMAS NMR spectroscopy. At low zinc concentrations (<0.15 Zn/Al) the cations are preferentially incorporated in the vicinity of two framework aluminum atoms. With increasing zinc loading ($0.15 \leq Zn/Al \leq 0.26$), additional cation sites are created at nearby framework aluminum pairs with two zinc cations being bridged by an oxygen atom. At higher zinc loading ($0.26 < Zn/Al < 0.77$) zinc oxide is formed in addition to the other two Zn^{2+} species.

1. Introduction

Zeolites are widely used as catalysts in organic syntheses[1] and petrochemical processes.[2] Their properties and, thus, their performance as catalysts can be subtly adjusted by modification with metal cations. Zinc-loaded zeolites, in particular, are suitable catalysts for the Heck reaction,[3] propane aromatization,[4] dehydrogenation of small paraffins,[5] hydroamination,[6−8] aromatization of in situ generated ethylene,[9] and the hydration of acetylene.[10,11] Understanding the nature and the location of Zn cations at specific sites is required for controlling activity and selectivity of such catalysts.[12] Therefore, controlled preparation and detailed characterization, in particular the identification of ion exchange positions for Zn^{2+}, is crucial.

Particularly interesting in this respect is zeolite BEA, which is frequently utilized in organic syntheses catalyzing, e.g., the acylation of aromatics[13] and the Meerwein−Pondorf−Verley reaction.[14,15] The high catalytic activity frequently observed for zeolite BEA might be related to its open pore structure and its high defect concentration.[16,17] The main channel system consists of 12-membered rings of oxygen atoms. Two straight channels are present in the [100] and [010] directions and a third sinusoidal 12-ring channel is located parallel to the [001] direction. These large pore channels intersect leading to the very open structure. The secondary building units consist of 6-, 5-, 4-membered-ring cages, each of them facing with at least one side to a 12-membered-ring channel. In consequence, a variety of possible coordination sites for the zinc cations exists.

Here, we report the successful synthesis and physicochemical characterization of zinc-exchanged zeolite BEA, utilized as catalyst for hydroamination reactions,[6,7] by means of molecular probes, combined with structural information obtained from EXAFS, NMR, and structural modeling.

2. Experimental Section

2.1. Zinc Ion Exchange. Zeolite H-BEA (Südchemie AG, T-4546, MA039 H/99, Si/Al 11.6, average crystal size 0.1−0.2 μm) was suspended in an aqueous solution of zinc acetate (0.08−0.55 M). The suspension was stirred for 14 to 93 h at 80 °C. The solid was separated by centrifugation, washed several times with distilled water, dried at 40 °C and calcined in a flow of air (100 mL/min, for experimental details see Table 1). The chemical composition was determined by AAS (Table 1).

2.2. IR Spectroscopy. IR spectra were obtained on a Bruker FTS 88 spectrometer equipped with a MCT detector. The samples were prepared as self-supporting wavers of approximately 10 mg/cm^2 density. The wavers were placed in a vacuum cell equipped with CaF_2 windows and activated ($p < 10^{-4}$ Pa, $T = 30$ to 450 °C at 10 °C/min and 1 h at 450 °C). Acetonitrile-d_3 was adsorbed with a partial pressure of 10 Pa at 35 °C for 15 min; pyridine was adsorbed with a partial pressure of 1 Pa at 100 °C for 1 h. The samples were outgassed for 1 h at the temperatures stated in the text. Deuterium oxide (Aldrich) was adsorbed with a partial pressure of 50 Pa at 100 °C and the sample was subsequently outgassed at 400 °C (100 to 400 °C at 10 °C/min). The IR spectra were recorded at 4-cm^{-1} resolution, baseline corrected, and normalized to the intensities of the overtones of skeletal vibrations in the region between 2115 and 1753 cm^{-1}. Difference spectra were calculated by subtracting the spectrum of the activated zeolite from the spectra of the zeolite in contact with the adsorbed probe molecules.

* Address correspondence to this author. E-mail: johannes.lercher@ch.tum.de.
[†] Technische Universität München.
[‡] Federal Institute of Technology (ETH).

10.1021/jp0373043 CCC: $27.50 © 2004 American Chemical Society
Published on Web 03/09/2004

TABLE 1: Preparation of Zn/H-BEA and Chemical Composition of the Samples[a]

sample	$Zn(CH_3CO_2)_2$ (mol/L)	soln/zeolite (mL/g)	no. of repetitions	total time of exchange (h)	calcination method	Al content (mmol/g)	Si/Al	Zn content (mmol/g)	Zn/Al	Zn/unit cell
H-BEA						1.36	11.6			
Zn/H-BEA	0.01	5	1	93	A	1.37	11.4	0.03	0.02	0.1
Zn/H-BEA	0.02	5	1	14	A	1.27	12.6	0.06	0.04	0.2
Zn/H-BEA	0.03	5	1	14	A	1.47	10.7	0.11	0.08	0.4
Zn/H-BEA	0.06	5	1	45	B	1.37	11.3	0.20	0.15	0.8
Zn/H-BEA	0.06	5	2	69	B	1.18	13.4	0.31	0.26	1.2
Zn/H-BEA	0.06	5	3	163	B	1.21	12.7	0.49	0.40	1.9
Zn/H-BEA	0.06	5	4	189	B	1.18	12.7	0.54	0.46	2.2
Zn/H-BEA	0.38	5	4	131	B	1.24	12.0	0.66	0.53	2.6
Zn/H-BEA	0.55	7	4	96	A	1.12	12.1	0.86	0.77	3.8

[a] Calcination method A: rt to 120 °C, 0.5 °C/min; 120 °C, 3 h; 120−500 °C, 1 °C/min; 500 °C, 2 h. B: rt to 500 °C, 5 °C/min; 500 °C, 5 h.

For acetonitrile-d_3, the difference spectra were baseline corrected in the region of the CN vibrations (2350−2200 cm^{-1}) and the intensities of the individual bands in this region calculated after deconvolution of the CN stretching vibrations (using 0.5 Gaussian and 0.5 Lorentzian contributions).

2.3. Temperature-Programmed Desorption (TPD) and Microbalance Experiments. TPD experiments were performed in a custom-built apparatus consisting of a quartz sample tube connected to a vacuum system. An ca. 80−100 mg sample was placed in the quartz tube and activated ($p = 10^{-2}$ Pa, $T = 30$ to 450 °C at 10 °C/min and 1 h at 450 °C). Acetonitrile (Aldrich), ammonia (Aldrich), and 2-propylamine (Aldrich) were adsorbed at 100 Pa for 15 min and the sample was outgassed at 10^{-2} Pa for 1.5 and 3 h, respectively. Subsequently, the temperature was increased at 10 °C/min and the rate of desorption followed by mass spectrometry. The intensity of the MS signals was normalized to the sample mass and each data series analyzed, using *m*/*z* 16 for ammonia, 41 for acetonitrile, 41 for propene, and 44 for 2-propylamine. Corresponding microbalance experiments were performed on a Setaram microbalance following the same experimental procedure.

2.4. In situ X-ray Absorption Spectroscopy. The local environment and the oxidation state of zinc cations were studied by X-ray absorption spectroscopy at the Zn K-edge. The spectra were collected at the beam-line ×1 at HASYLAB, DESY Hamburg, using a double crystal Si (111) monochromator. The samples were prepared as self-supporting wafers choosing the weight to achieve a total absorption of $\mu x = 2.5$ (around 200 mg). The wafers were placed in a sample holder equipped with a heating and cooling system, which was placed in a stainless steel reactor with Capton windows. The samples were activated in a stream of He (65 mL/min, room temperature to 450 °C at 10 °C/min; 1 h at 450 °C).

Spectra were recorded at liquid nitrogen temperature before (in the case of Zn/H-BEA 0.08 Zn/Al) and after activation. The spectra were analyzed with WinXas (Version 2.0).[18] The energy of the spectra was calibrated to the first inflection point of the K-edge from a simultaneously measured zinc foil ($E_0 = 9659$ eV). The background was corrected and normalized by fitting the preedge region with a second-order polynom and the section above the edge by a polynomial spline with seven nodes. The oscillations were Fourier transformed in the range $k = 2.1-16$ $Å^{-1}$, using k^2 weighting. The local environment of the zinc atoms was determined from the EXAFS by fitting in *k*-space, using phase-shift and amplitude functions for Zn−O and Zn−Zn calculated assuming multiple scattering processes (FEFF Version 8.10).[19]

2.5. Structure Simulation. A cluster consisting of 35 T-atoms (terminated with −OH groups) was isolated from the crystallographic structure of zeolite BEA and used to calculate the energetic contributions and geometry of Zn^{2+} cations at different ion exchange positions of BEA, using the density functional theory (DFT) approach. The cluster was sufficiently large to allow exploring all ion exchange positions. The geometry was optimized with respect to the energy, using a double numerical basis set. After geometry optimization had been achieved, the final energy was calculated, using the exchange correlation based on the Becke, Lee, Yang, Parr method (BLYP). The program DMol3 was used for the theoretical calculations.[20] Zn^{2+} cations were placed at 4-MR, 5-MR, and 6-MR positions and, for each of the geometries, two Si^{4+} atoms were replaced by Al^{3+} to maintain the neutral charge of the cluster. To account for the different energies for the Al^{3+} substitution the charge was balanced with two protons and the energy also calculated for each of the geometries. The stability of the Zn^{2+} cations at a particular position was then determined from the difference in energy.[21]

2.6. ^{27}Al MAS and MQ MAS NMR Spectroscopy. ^{27}Al MAS and 3Q-MAS NMR experiments were carried out on a Bruker AMX-400 FT-NMR spectrometer at a magnetic field of 9.4 T, using a 4-mm CP-MAS probe-head. The radio frequency pulse length for the ^{27}Al MAS experiments was 0.6 μs, equal to a $\pi/8$ pulse. A spinning frequency of 12 kHz and a recycle delay of 1 s were employed for the ^{27}Al MAS NMR experiments and 2000 scans were accumulated. The ^{27}Al 3Q-MAS experiments were performed with a three-pulse sequence incorporating a *z*-filter at a spinning speed of 12 kHz. An radio frequency field of 106 kHz was used for the creation and the first conversion pulses. These pulses were individually optimized. For the last conversion step, which is the central transition selective soft 90° pulse, a radio frequency field of 24 kHz was used. A 2D Fourier transformation followed by a shearing transformation gave a pure absorption mode 2D contour plot. ^{27}Al chemical shifts were referenced to $(NH_4)Al(SO_4)_2 \cdot 12H_2O$. Quantification of the aluminum resonances was done by a computer fitting of the corresponding 1D MAS spectra, using the quadrupolar parameters determined from the 3Q-MAS experiments.

3. Results

3.1. Overall Acid Site Concentration. The overall concentration of acid sites in Zn/H-BEA samples was determined by ammonia adsorption/desorption, using temperature programmed desorption (TPD). Deconvolution of the TPD traces revealed desorption peaks with maxima at 233, 320, and 452 °C denoted α-, *β*-, *γ*-states (see Figure 1 for Zn/H-BEA 0.53 Zn/Al). Desorption was a purely first-order process (independence of the peak maximum on the concentration of ammonia adsorbed) and desorption maxima were confirmed by TPD experiments after outgassing at progressively elevated temperatures to

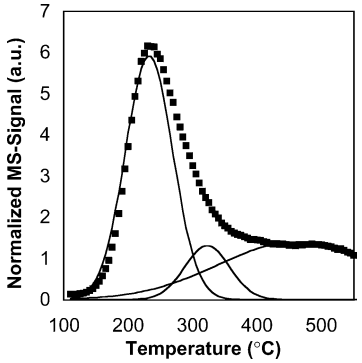

Figure 1. TPD of ammonia from Zn/H-BEA (0.53 Zn/Al) (■, observed TPD trace; —, contributions of specific sites).

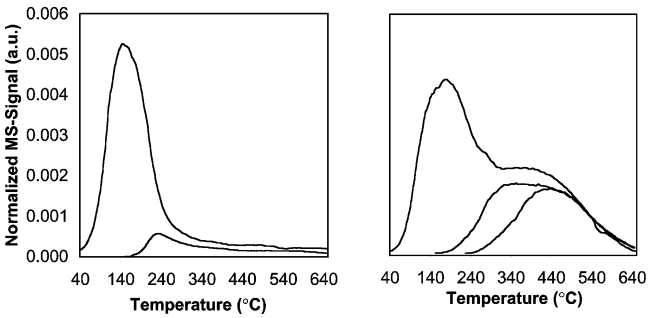

Figure 2. TPD of acetonitrile from H-BEA (left, for adsorption at 40 and 150 °C) and Zn/H-BEA (0.53 Zn/Al, right, for adsorption at 40, 150, and 220 °C).

remove the weaker adsorbed ammonia. From the total amount of ammonia adsorbed on the parent H-BEA zeolite a total acid site concentration of 0.46 mmol/g was calculated. With increasing zinc content the value increased linearly to 0.93 mmol/g at 0.53 Zn/Al.

The contribution of individual desorption states as a function of the zinc loading was obtained by deconvolution. The concentration of the β-state decreased from 0.14 to 0.07 mmol/g in the range 0−0.04 Zn/Al and remained constant at higher zinc loadings. In contrast, the concentration of the α- and the γ-state increased continuously with the zinc loading. The β-state is, therefore, attributed to Brønsted acid sites, whereas the α- and the γ-state are assigned to at least two different Lewis acid sites which increase in concentration upon Zn^{2+} incorporation. It should be emphasized that the presence of other acid sites in these materials may contribute to the three main peaks. Therefore, a more detailed characterization of the material was required.

3.2. TPD of Acetonitrile. In contrast to ammonia, acetonitrile binds preferentially to zinc cations showing only weak interactions with Brønsted acid sites.[22] Thus, TPD of acetonitrile monitors primarily the changes in the nature and concentration of Zn^{2+} Lewis acid sites. As an example, the TPD curves of acetonitrile from H-BEA and Zn/H-BEA (0.53 Zn/Al) at different outgassing temperatures are compiled in Figure 2.

The rate of acetonitrile desorption from the parent H-BEA had only one maximum at 156 °C. As acetonitrile interacts only weakly with Brønsted acid sites, the desorption maximum indicates that Al^{3+} Lewis acid sites have formed during activation.

The TPD curves of the Zn/H-BEA samples exhibited marked variations. At a low zinc loading (0.08 Zn/Al), the TPD curve also had a maximum at 156 °C with a shoulder ranging from 240 to 600 °C. The coincidence of the peak at 156 °C with that in H-BEA together with its lower intensity led us to conclude

TABLE 2: Concentration of Zinc Sites in Zn/H-BEA (0.53 Zn/Al) as Determined by Adsorption of Acetonitrile

	desorption temp (°C)	amount of CH_3CN adsd (mmol/g)
zinc site A	176	0.20
zinc site B	359	0.13
zinc site C	456	0.33

that the concentration of Al^{3+} Lewis acid sites decreases upon Zn^{2+} cation exchange. The shoulder at higher temperatures is attributed to desorption of acetonitrile from Zn^{2+} cations.

At a higher Zn^{2+} loading (0.53 Zn/Al), the first peak broadened, decreased in intensity, and shifted to 176 °C, while the intensity of the shoulder increased considerably. The differing halfwidth and the increase in the temperature of the desorption maximum indicates that for Zn/H-BEA (0.53 Zn/Al) this desorption state is related to Zn^{2+} cations (Zn^{2+} based Lewis acid sites; Zn^{2+} site A) and is not based on Al^{3+} Lewis acid sites. As for Zn/H-BEA (0.08 Zn/Al) above, the shoulder ranging from 240 to 600 °C is also attributed to acetonitrile strongly adsorbed on Zn^{2+} cations.

In summary, TPD of acetonitrile on samples with low zinc loading indicates desorption of CH_3CN from Al^{3+} and Zn^{2+} Lewis acid sites at 156 and 240−600 °C, respectively. Increase of the zinc loading up to 0.53 Zn/Al led to the formation of a new desorption maximum of acetonitrile at 176 °C, while the desorption from Al^{3+} Lewis acid sites was not observed. The shoulder ranging from 240 to 600 °C is attributed to acetonitrile strongly adsorbed on Zn^{2+} cations located at not less than two different sites in the zeolite.

To assess the number of sites, TPD experiments were performed at different adsorption and outgassing temperatures. Subtraction of the TPD curve obtained at higher equilibration temperature from the TPD curve obtained at lower temperatures provided two further maxima at 359 and 456 °C (Zn^{2+} site B and C).

The concentration of acetonitrile adsorbed on these sites was determined by means of microgravimetry. At an equilibration temperature of 220 °C, adsorption occurred only on zinc site C (see Figure 2). In this case, the total concentration of CH_3CN adsorbed was 0.33 mmol/g (Zn/H-BEA 0.53 Zn/Al) and the ratio of adsorbed CH_3CN molecules to Zn^{2+} cations was 0.5. This indicates that half of the zinc cations interact with acetonitrile.

At an equilibration temperature of 150 °C, CH_3CN adsorbed only on sites B and C, whereas adsorption on Zn^{2+} site A sites (176 °C) was negligible. The overall CH_3CN concentration adsorbed on the sample at this temperature was 0.46 mmol/g. The ratio of adsorbed CH_3CN to Zn^{2+} cations was 0.7. With the concentration of Zn^{2+} in site C (0.33 mmol/g), the concentration of Zn^{2+} in site B was 0.13 mmol/g. Assuming the formation of a 1:1 complex between acetonitrile and zinc cations, the concentration of zinc site A is then calculated to be 0.20 mmol/g.

3.3. TPD of 2-Propylamine from Zinc-Exchanged BEA Zeolites. TPD of reactive probe molecules, such as 2-propylamine, has been proposed to be suitable for differentiating between Brønsted and Lewis acid sites in H-zeolites.[23] Brønsted acid sites catalyze the decomposition of chemisorbed 2-propylamine to ammonia and propene (Hoffmann elimination,[24−26] eq 1), while 2-propylamine adsorbed on other sites is claimed to desorb molecularly. Because of the strong chemisorption of amines at Zn^{2+} cations we would expect that 2-propylamine

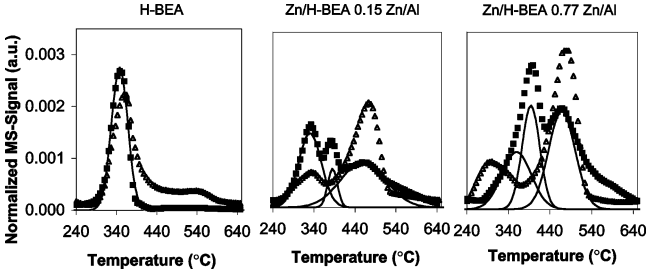

Figure 3. TPD of chemisorbed 2-propylamine desorbing as propene (■) and ammonia (△). The TPD trace of propene was deconvoluted and the contributions of single sites are shown (—).

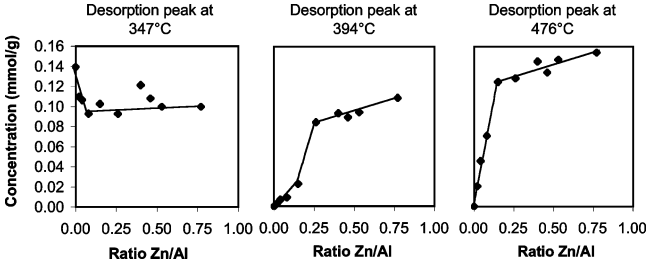

Figure 4. Quantification of different sites in Zn/H-BEA zeolites determined from the propene desorption in 2-propylamine TPD. The desorption peak at 347 °C is attributed to Brønsted sites, the peaks at 394 and 476 °C to zinc sites.

desorbing from Zn^{2+} cations also decomposes to ammonia and propene (reverse hydroamination, eq 2).

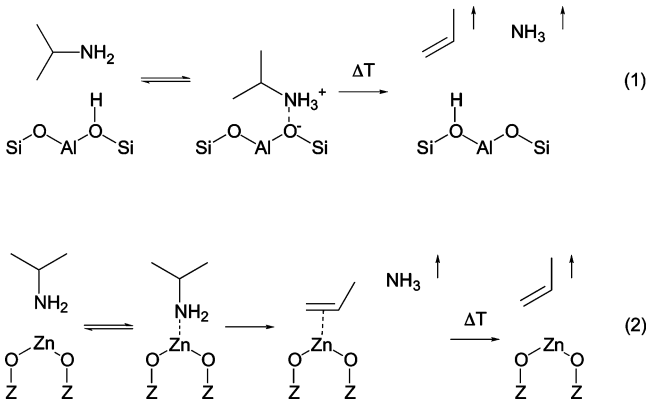

For the present series of Zn/H-BEA zeolites TPD of 2-propylamine after equilibration at 40 °C at a pressure of 0.1 Pa was followed by mass spectrometry. All samples showed a broad desorption peak of 2-propylamine below 260 °C attributed to desorbing physisorbed molecules. For H-BEA, propene desorption started at 290 °C and reached a maximum at 347 °C. Ammonia started to desorb in parallel to propene at 290 °C (see eq 1). However, the maximum of desorption rate was found at slightly higher temperatures (365 °C) and the integral intensity of the desorption peak was lower compared to that of propene. Additional ammonia desorbed in a broad shoulder from 420 to 620 °C. This fraction of ammonia is tentatively attributed to readsorption of ammonia on Lewis acid sites formed during TPD and its subsequent release at higher temperatures. The assignment is supported by TPD of NH_4^+ ion exchanged H-BEA showing also a peak at 452 °C, which is assigned to the desorption of ammonia from strong Lewis acid sites.

Upon heating 2-propylamine chemisorbed on Zn/H-BEA also decomposed to ammonia and propene, but showed a drastically different evolution of propene and ammonia. The rate of propene desorption had maxima at 347, 394, and 476 °C (Figure 3). Comparison with TPD from parent H-BEA indicates that propene desorption at 347 °C is related to Hoffmann elimination on Brønsted acid sites. This desorption state exists in all zinc-exchanged samples. The desorption states of propene at 394 and 476 °C are attributed to two different zinc sites.

In contrast to the decomposition on H-BEA, ammonia did not desorb in parallel to propene from Zn/H-BEA. The onset of the ammonia evolution decreased with the Zn^{2+} content of the zeolite from 270 to 240 °C. In contrast, the start of the propene desorption remained roughly at 270 °C. This is contra expectation as ammonia, which is the stronger base relative to propene, would interact more strongly with the zinc Lewis acid sites of the zeolite. However, this observation confirms that zinc-exchanged BEA zeolites catalyze hydroamination reactions, which are reverse to the decomposition of propylamine. Mechanistically initial coordination of the CC π system to the metal center followed by reaction with an approaching amine molecule was invoked for hydroamination.[27] In the reverse reaction the amine should, due to microreversibility, be released first. With increasing Zn^{2+} concentration the first maximum of ammonia desorption shifted from 365 to 260 °C, suggesting decreasing acid strength with increasing concentration of Zn^{2+}. Because of its variation in intensity in parallel to the propene desorption peak at 394 °C, we attribute it to decomposition on propylamine decomposition on strong Brønsted acid sites.

The second ammonia peak at 480 °C increased with the Zn^{2+} concentration. This peak occurred in parallel to the desorption peak of propene at 476 °C, indicating that propylamine decomposition must have occurred with Zn^{2+} cations involved. However, the ammonia peak at 480 °C had a significantly higher intensity than that for propene. Thus, in analogy to the interpretation of the high-temperature shoulder observed with H-BEA, we propose that the higher intensity is related to desorption of ammonia originating from the decomposition at Brønsted acid sites and subsequent trapping at Zn^{2+} Lewis acid sites. It should be emphasized at this point that the TPD peaks observed are related in all cases to the elementary steps of decomposition and the chromatographic adsorption−desorption as the products evolve from the zeolite bed.

To empirically follow the variations of the reactivity induced by the various levels of Zn^{2+} the TPD curves of propene were deconvoluted, using three discrete contributions with maxima at 374, 394, and 476 °C (see Figure 3). The integrated areas of the three peaks as a function of the zinc loading are given in Figure 4.

The desorption peak at 347 °C attributed to Brønsted acid sites decreased in intensity in the range 0−0.08 Zn/Al and remained constant at higher Zn^{2+} concentrations. The desorption peaks at 394 and 476 °C, both assigned to Lewis acid sites, complement each other. The intensity of the desorption peak at 476 °C increased rapidly up to 0.15 Zn/Al, whereas only a small increase in the concentration of the peak at 394 °C was observed. Between 0.15 and 0.26 Zn/Al, the intensity of the desorption peak at 476 °C increased slightly, while a sudden rise in the intensity of the peak at 394 °C was observed. At even higher Zn^{2+} concentrations, the intensity of both peaks increased gradually. This indicates that the desorption maxima at 476 and 394 °C correspond to two different Zn^{2+} sites. A third type of Zn^{2+} site must be present at concentrations above 0.26 Zn/Al. It was, however, not observed in 2-propylamine TPD. Therefore, we conclude that this type does not catalyze the decomposition of 2-propylamine.

Note that these observations are in good agreement with the results from acetonitrile TPD, which had shown that three types

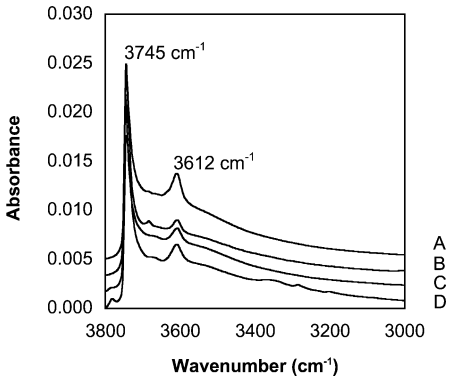

Figure 5. IR spectra of zinc-exchanged BEA zeolites with various zinc loadings. The spectra were recorded after activation at 450 °C (spectra A to D for Zn/H-BEA 0.77, 0.40, and 0.04 Zn/Al and H-BEA, respectively).

of Zn^{2+} Lewis acid sites are present in Zn/H-BEA (0.53 Zn/Al). TPD of acetonitrile led to peaks at 176, 359, and 456 °C attributed to desorption from zinc sites A, B, and C, respectively. By TPD of 2-propylamine two Zn^{2+} sites were identified showing propene desorption at 394 and 476 °C. On the basis of the relative intensities of the propene peaks at 394 and 476 °C these desorption states are attributed to zinc sites B and C, respectively. We conclude that zinc site A corresponds to Zn^{2+} sites that adsorb 2-propylamine only weakly so that it desorbs before reacting.

3.4. IR Spectroscopy of Zn/H-BEA. The IR spectra of BEA zeolites with various zinc loadings are compiled in Figure 5. The most prominent band of the OH stretching vibrations at 3745 cm^{-1} is attributed to terminal silanol groups of the zeolite. The band at 3612 cm^{-1} is attributed to OH groups associated with isolated Brønsted acid sites. A broad band (3750−3200 cm^{-1}) with a maximum at approximately 3500 cm^{-1} was observed in all spectra. In accordance with the literature this band is assigned to OH groups involved in hydrogen-bonding interactions.[28,29] Additionally, two bands with low intensity were noted. The band at 3780 cm^{-1}, frequently assigned to hydroxyl groups on extraframework aluminum oxide, was only observed in the spectra of the parent H-BEA zeolite and, in much smaller intensity, for Zn/H-BEA 0.04 Zn/Al. Apparently, these hydroxyl groups are removed during the zinc ion exchange.[28,30] The band at 3660 cm^{-1} is assigned to OH groups coordinated to aluminum or mixed oxide clusters in the zeolite pores. This band was observed with the parent H-BEA zeolite and with two higher exchanged zeolites (0.40 and 0.46 Zn/Al).

From the constant intensity of the band at 3745 cm^{-1} we conclude that Zn^{2+} cation exchange did not influence the concentration of SiOH groups. The concentration of isolated Brønsted acid sites (3612 cm^{-1}) decreased slightly with the Zn^{2+} content (0−0.15 Zn/Al), whereas at higher loading their concentration increased. The variations in the intensity of the 3612-cm^{-1} band were so small that it was concluded that also these Brønsted acid sites are hardly affected by zinc ion exchange. The concentration of the Brønsted sites involved in hydrogen bonding (3750−3200 cm^{-1}) was not quantified, as hydrogen bonding interactions lead to marked changes in the molar extinction coefficients of the OH bands.[31]

The accessibility of these OH groups was explored by H/D exchange with D_2O. After exposure of H-BEA and Zn/H-BEA (0.15 Zn/Al) to D_2O all OH bands shifted to lower wavenumbers. The bands formed between 2820 and 2400 cm^{-1} mirrored precisely the bands between 3780 and 3050 cm^{-1}, indicating that all OH groups in zeolite BEA were converted to OD groups and, hence, are accessible.

3.5. IR Spectroscopy of Adsorbed Acetonitrile-d_3. The relative concentration of Lewis and Brønsted acid sites was assessed from the IR spectra of adsorbed acetonitrile-d_3.[32,33] After adsorption of CD_3CN, the bands of OH stretching vibrations at 3745 and 3612 cm^{-1} decreased in intensity. While the band at 3745 cm^{-1} regained its original intensity almost completely after outgassing, the band at 3612 cm^{-1} did not. This shows that acetonitrile molecules interact weakly with SiOH groups, while the interaction with the isolated Brønsted acid sites is much stronger. In contrast, the intensity of the broad underlying band between 3750 and 3200 cm^{-1} did not change significantly. Thus, hydrogen-bonded OH groups do not interact with acetonitrile-d_3. This is attributed to the low basicity of acetonitrile, which is insufficient to break existing O−H···O hydrogen bonds.[34]

In the gas phase, acetonitrile-d_3 has an intense ν_{st}(C≡N) band at 2594 cm^{-1}, which is shifted significantly upon adsorption. On the parent H-BEA zeolite a cluster of four overlapping bands at 2323, 2298, 2273, and 2250 cm^{-1} was observed. These are attributed to interaction of the nitrile group with Al^{3+} Lewis acid sites (Al LAS), Brønsted acid sites (BAS), SiOH groups, and the asymmetric stretching vibration of physisorbed CD_3-CN, respectively.[32,35] For zinc-exchanged zeolites an additional band was observed at 2314 cm^{-1}, which increased in intensity with the Zn^{2+} loading (see Figure 6, left). In parallel, the band at 2323 cm^{-1} due to interaction with Al^{3+} Lewis acid sites decreased. For all samples, the fraction of acetonitrile-d_3 molecules adsorbed on silanol groups was negligible. The contribution of each band was then determined by deconvolution (see Figure 6, right, for Zn/H-BEA Zn/Al 0.08).

The concentrations of the Al^{3+} Lewis and Brønsted acid sites in the material were calculated with the extinction coefficients 3.62 ± 0.16 and 2.05 ± 0.10 cm/μmol, respectively.[36] The concentration in Zn^{2+} Lewis acid sites was estimated by using the extinction coefficient for Al^{3+} Lewis acid sites. The concentration of Brønsted acid sites decreased from 0.14 (H-BEA) to 0.11 mmol/g (Zn/H-BEA 0.04 Zn/Al) and remained constant at Zn^{2+} concentrations (Figure 7). The concentration of Al^{3+} Lewis acid sites decreased linearly from 0.27 (H-BEA) to 0 mmol/g (Zn/H-BEA 0.26 Zn/Al). As to be expected, the intensity of the band characteristic for Zn^{2+}-based Lewis acid sites increased in parallel with the zinc concentration in the material.

The trend can be divided into three sections of linear increase differing in slope. The increase in intensity was similar in the range 0−0.15 Zn/Al and 0.15−0.26 Zn/Al, whereas the increase related to the amount of Zn^{2+} in the zeolite was considerably lower at higher zinc loadings. These observations indicate that three different zinc phases with different accessibility for acetonitrile are present in the material.

It is particularly noteworthy that in the range 0−0.26 Zn/Al the linear decrease in the concentration of Al^{3+} Lewis acid sites correlated inversely with the intensity of the band characteristic for Zn^{2+}-based Lewis acid sites. Therefore it is necessary to analyze the correlation with respect to possible surface reactions. Vicinal Brønsted acid sites are thermally unstable and dehydroxylate easily forming an Al^{3+} Lewis site.[32,37] This suggests that ion exchange with Zn^{2+} leads to the stabilization of aluminum in the lattice or to the replacement of Al^{3+} Lewis sites by Zn^{2+}. As the Si/Al ratio did not change to the extent that leaching of Al^{3+} can be inferred, we conclude that the divalent zinc cations preferentially exchange at sites that have

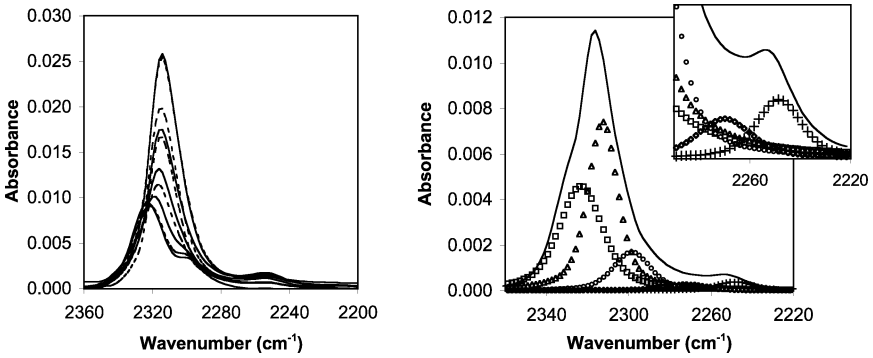

Figure 6. IR spectra of acetonitrile-d_3 adsorbed on zinc-exchanged BEA zeolites (left, form top to bottom: Zn/H-BEA 0.77, 0.53, 0.46, 0.40, 0.26, 0.16, 0.08, 0.04, 0.02 Zn/Al and H−BEA) and the contribution of individual sites shown for Zn/H-BEA 0.08 Zn/Al (right, −, observed TPD trace; □, 2323 cm^{-1} Al LAS; △, 2314 cm^{-1} Al LAS; ○, 2298 cm^{-1} BAS; ◇, 2273 cm^{-1} Silanol groups; +, 2240 cm^{-1} physisorbed acetonitrile-d_3).

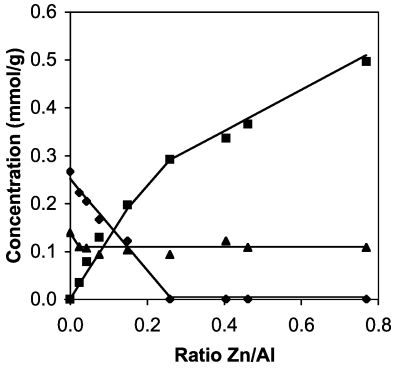

Figure 7. Concentration of Brønsted acid, Al^{3+} Lewis acid, and zinc sites in Zn/H-BEA in dependence of the zinc loading (obtained by quantification of the IR spectra of adsorbed acetonitrile-d_3) (◆, Al LAS; ■, zinc sites; ▲, BAS).

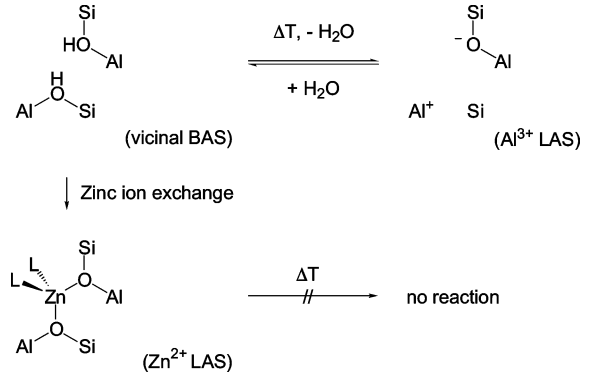

Figure 8. Dehydroxylation reactions postulated for Zn/H-BEA at low zinc ion exchange degree (L = framework oxygen or neutral ligand).

two Al^{3+} cations in the lattice vicinity. This relation can be quantified (eq 3) assuming that (i) isolated Brønsted acid sites

$$c_{AS}^{tot} = c_{BAS} + 2c_{Zn\ site} + 2c_{Al\ LAS} \qquad (3)$$

are thermally stable, (ii) Zn^{2+} exchanges preferentially at vicinal Brønsted acid sites, and (iii) these Brønsted acid sites dehydroxylate forming one Al^{3+} Lewis acid site, if not stabilized by Zn^{2+} (see Figure 8).

TPD of 2-propylamine suggested that the concentration of isolated Brønsted acid sites c_{BAS} was approximately constant over the whole range of zinc exchange. In the range 0−0.26 Zn/Al, the concentration of zinc cations in the material was inversely proportional to the decrease of Al^{3+} Lewis acid sites. Consequently, the total concentration of acid sites calculated according to eq 3 was approximately constant in the range 0−0.26 Zn/Al (Table 3). For materials with higher Zn^{2+} loading, the total concentration of acid sites increased linearly with the Zn^{2+} content. Thus, at low zinc concentrations the zinc cations preferentially exchange at vicinal Brønsted acid sites (<0.26 Zn/Al). At a zinc content of 0.26 Zn/Al, all pairwise located Brønsted acid sites are stabilized by one zinc cation. In materials with higher Zn^{2+} concentration, vicinal Brønsted acid sites are not available for all cations so that other forms of incorporation must exist (see discussion below).

3.6. IR Spectroscopy of Adsorbed Pyridine. Pyridine adsorbed on Brønsted acid sites shows a characteristic band at 1546 cm^{-1} (ϵ_{BAS} = 1.3 cm/μmol), whereas the interaction with Lewis acid sites leads to a characteristic band at 1456 cm^{-1} (ϵ_{LAS} = 1.5 cm/μmol).[28] For pyridine adsorbed on H-BEA both bands were observed after evacuation at 100 °C, confirming the presence of Brønsted and Lewis acid sites (Figure 9, left). For the Zn/H-BEA samples the intensity of the band at 1456 cm^{-1} increased linearly with the Zn^{2+} concentration. This indicates that pyridine adsorbs similarly on Al^{3+} and Zn^{2+} Lewis acid sites. The concentration of pyridinium ions formed decreased with the Zn^{2+} loading in the range from 0 to 0.08 Zn/Al and stayed constant with further zinc incorporation.

After evacuation at 450 °C, the concentration of pyridinium ions decreased to approximately a third of the value observed after evacuation at 100 °C, but the bands varied in a similar fashion with the concentration of Zn^{2+} (Figure 9, right). The concentration of pyridine adsorbed on Lewis acid sites of the parent H-BEA zeolite (0.15 mmol/g) was approximately 20% lower compared to the concentration after outgassing at 100 °C (0.19 mmol/g). For the Zn/H-BEA samples, the concentration of pyridine adsorbed on Lewis acid sites was constant up to 0.26 Zn/Al and increased at higher loadings. Thus, at least two different types of strong Zn^{2+} Lewis acid sites must exist, which is consistent with the observations described for the other techniques.

3.7. ^{27}Al MAS NMR Spectroscopy. These conclusions are supported by ^{27}Al MAS experiments. The spectrum of the parent H-BEA zeolite showed two distinct maxima at 53.4 and −1.1 ppm and a broad shoulder centered at 28 ppm (Figure 10). Deconvolution based on the peak positions resolved in the two-dimensional 3Q-MAS NMR spectrum of the same sample showed that in total five different species contribute to the one-dimensional spectrum (Table 4).[38] The two maxima can be assigned to aluminum atoms in tetrahedral (with isotropic shift 60.5, 55.1, and 42.5 ppm) and octahedral environment (with isotropic shift 1.4 and 1.5 ppm). It is especially noteworthy that two octahedral aluminum species with a large and a small

TABLE 3: Chemical Analysis of Zinc-Exchanged Zeolites and Quantitative Evaluation of IR and TPD Measurements (in mmol/g)

	AAS			IR CD_3CN			TPD of 2-propylamine		IR pyridine
sample	Zn	Al	Zn/Al	Al-Lewis sites	Zn-Lewis sites	total acid site concn[a]	Zn on close Al pairs[b]	Zn on nearby Al pairs[b]	Lewis acid sites[c]
H-BEA	0.00	1.36	0.00	0.27	0.00	0.67	0.00	0.00	0.15
Zn/H-BEA	0.03	1.37	0.02	0.22	0.04	0.62	0.02	0.003	
Zn/H-BEA	0.06	1.27	0.04	0.20	0.08	0.67	0.05	0.007	0.12
Zn/H-BEA	0.11	1.47	0.08	0.17	0.13	0.68	0.07	0.009	0.14
Zn/H-BEA	0.20	1.37	0.15	0.12	0.20	0.74	0.12	0.02	0.13
Zn/H-BEA	0.31	1.18	0.26	0.00	0.29	0.68	0.13	0.08	0.15
Zn/H-BEA	0.49	1.21	0.40	0.00	0.34	0.79	0.15	0.09	
Zn/H-BEA	0.54	1.18	0.46	0.00	0.37	0.84	0.13	0.09	0.20
Zn/H-BEA	0.66	1.24	0.53	0.00			0.15	0.09	0.27
Zn/H-BEA	0.86	1.12	0.77	0.00	0.50	1.10	0.15	0.11	0.26

[a] Calculated from eq 3. [b] Desorbing propene in mmol/g. [c] Determined from the integral intensity at 1456 cm^{-1}, after outgassing at 450 °C for 1 h.

TABLE 4: Relative Peak Intensities in the ^{27}Al MAS NMR Spectra

	H-BEA		Zn/H-BEA 0.08 Zn/Al		Zn/H-BEA 0.26 Zn/Al	
	position (ppm)	rel int (%)	position (ppm)	rel int (%)	position (ppm)	rel int (%)
tetrahedral peak 1	60.5	20	61.1	19	58.2	24
tetrahedral peak 2	55.1	29	55.1	31	55.6	29
tetrahedral (broad)	42.5	35	47.2	37	53.2	39
octahedral 1	1.4	7	2.2	3	not observed	0
octahedral 2 (broad)	1.5	9	1.5	10	6.2	8

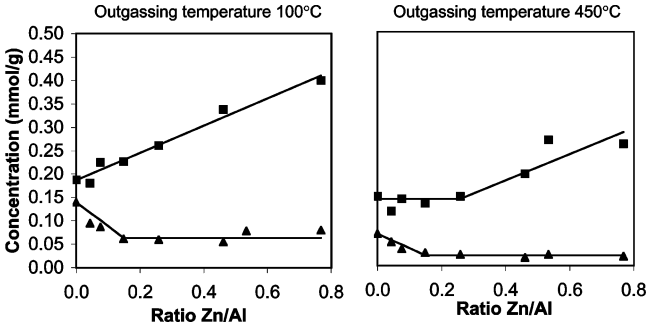

Figure 9. Concentration of Lewis (■) and Brønsted acid sites (▲) of Zn/H-BEA as a function of the zinc loading derived from IR spectra of adsorbed pyridine.

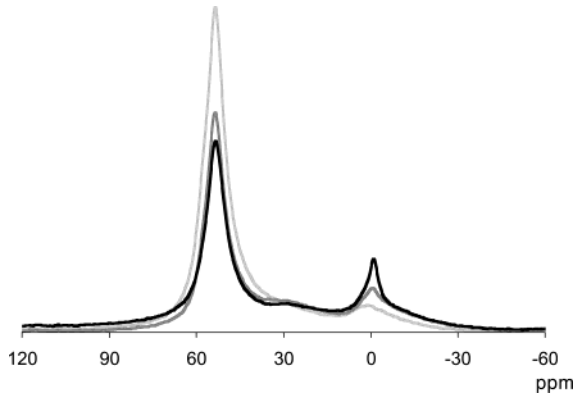

Figure 10. ^{27}Al NMR spectra of H-BEA (black) and Zn/H-BEA (0.08 and 0.26 Zn/Al, dark and light gray, respectively).

quadrupolar coupling constant can be distiguished (corresponding to a broad and a sharp signal in the one-dimensional NMR spectrum).

The concentration of the latter octahedral aluminum species decreased gradually with Zn exchange, and was exactly zero in the sample Zn/H-BEA 0.26 Zn/Al for which no Al^{3+} Lewis acid sites were observed in the IR spectrum of adsorbed acetonitrile-d_3. It is noteworthy that only the sharp octahedral peak is correlated to the zinc contents, but not the broad peak. In parallel to the decreasing concentration of octahedral aluminum sites, the concentration of tetrahedral aluminum sites increased. In consequence, the ratio of tetrahedral to octahedral aluminum species increased from 84:16 (H-BEA) to 87:13 (Zn/H-BEA 0.08 Zn/Al) and 92:8 (Zn/H-BEA with 0.26 Zn/Al). Note that the ^{27}Al NMR spectra were taken for a nonactivated, partially hydrated sample. The acid site concentrations can therefore not be directly compared to the IR and TPD data which were taken on actived, fully dehydrated samples. A detailed discussion is given below.

TABLE 5: Energies at the Zn K-Edge for Zn/H-BEA and Reference Material

sample	Zn/Al	oxidation state	edge energy (eV)	sample treatment
Zinc metal		Zn^0	9659.3	
ZnO		Zn^{2+}	9661.8	
Zn/H-BEA	0.08	Zn^{2+}	9663.5	before activation
Zn/H-BEA	0.08	Zn^{2+}	9663.0	after activation
Zn/H-BEA	0.53	Zn^{2+}	9663.1	after activation

3.8. X-ray Absorption Near-Edge Structure (XANES). The excitation of Zn 1s electrons causes a sharp increase in X-ray absorption near 9659 eV. The energy is a function of the electron density on the absorber atom and, conceptually, decreasing electron density leads to a shift of the edge to higher energies.[4,39] Therefore, a comparison of the edge positions of Zn^{2+}-exchanged zeolites with reference compounds (i.e., Zn and ZnO) allows us to estimate the average charge of incorporated zinc species. In Table 4, the edge energies of Zn/H-BEA (0.08 and 0.53 Zn/Al) before and after activation are compared with those of metallic Zn and ZnO.

The edge energy for zinc metal and ZnO was 9659.3 and 9661.8 eV, respectively. The change of the oxidation state from 0 to +2 is reflected in the shift of 2.5 eV to higher energies. For both Zn/H-BEA zeolites the edge was shifted to even higher energies (9663.0−9663.5 eV). This clearly indicates that zinc is present in a high oxidation state. Note that X-ray absorption spectroscopy determines the average charge of all zinc species present in the sample. The higher edge positions of the Zn/H-

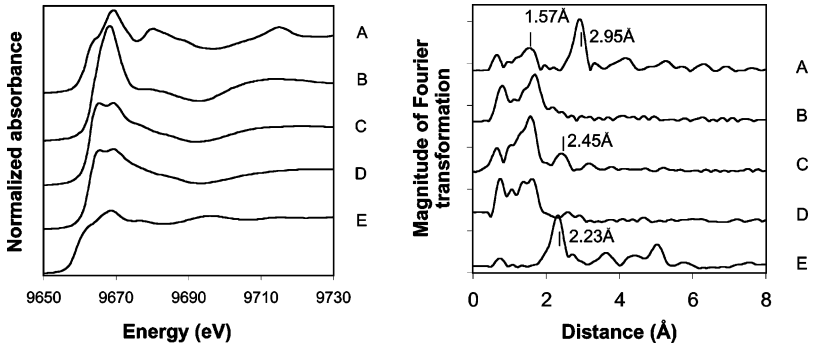

Figure 11. XANES (left) and EXAFS (right) at the Zn K-edge of (A) ZnO, (B) Zn/H-BEA 0.08 Zn/Al before activation, (C) Zn/H-BEA 0.08 Zn/Al after activation, (D) Zn/H-BEA 0.53 Zn/Al before activation, and (E) metallic zinc.

BEA samples compared to ZnO and the slight decrease in edge energy after activation (from 9663.5 to 9663.0 eV) results from differences in the coordination sphere of the zinc cations in the zeolite and the ZnO reference and from the loss of H_2O ligands during activation.

This is also confirmed by the Zn K-edge XANES of the zeolites investigated. For the fresh activated sample, the hydration of Zn^{2+} resulted in a marked peak above the absorption edge, while after activation two peaks were observed (Figure 11, left). This confirms that the coordination sphere of Zn^{2+} cations changes significantly during activation. In contrast, zinc oxide showed one marked peak above the absorption edge indicating a well-defined chemical structure. The X-ray absorption data on zinc-exchanged BEA zeolite (0.08 Zn/Al) showed the same dehydration−hydration sequence as reported by Iglesia et al.[4] for Zn/H-ZSM-5 (Zn/Al 0−0.19), indicating that similar zinc species might be present in both materials.

3.9. Extended X-ray Absorption Fine Structure (EXAFS). The EXAFS of the Zn/H-BEA samples was analyzed to examine whether specific Zn−O, O−Zn−O, or Zn−Zn interactions exist. The Fourier transformed EXAFS oscillations weighted with k^2 (not corrected for the phase shift) of the samples and reference materials (ZnO and Zn metal) are shown in Figure 11, right. (Note that in the non-phase-shift corrected radial distribution functions the peaks are generally shifted to smaller distances.[40]) In the radial distribution function of metallic Zn the peak at 2.23 Å corresponds to the Zn−Zn contribution of the first coordination sphere. Both zinc-exchanged zeolites did not show Zn−Zn contributions at this distance, which clearly indicates that zinc is not present in a reduced (metallic) state in the zeolite samples. The ZnO reference material exhibited a peak around 1.6 Å, which results from the contributions of the four nearest oxygen neighbors and a peak at larger distances around 2.95 Å, which is attributed to Zn−Zn contributions. On both zeolite samples the peak of the Zn−O contributions was observed, which indicates that Zn is surrounded by oxygen atoms at a distance similar to that in the Zn-oxide phase, while the Zn−Zn contributions at larger distance were not observed. The absence of (well defined) Zn−Zn contributions strongly indicates that the zinc atoms are located at isolated ion exchange positions and that ZnO nanoparticles are absent (or present in a very low concentration). In addition, activated Zn/H-BEA 0.08 Zn/Al showed a peak at a distance of 2.45 Å (located between the Zn−Zn contributions in metallic Zn and Zn-oxide), which was not present in samples with a higher zinc loading or before activation. This peak most probably corresponds to Zn−O contributions, which are only observed at a low zinc ion exchange degree. This indicates that (i) Zn^{2+} sites are better defined in samples with low ion exchange degrees and (ii) that zinc is incorporated on specific ion exchange positions. The observation that this peak is not present in the hydrated sample can be explained by the unspecific adsorption of water on the Zn^{2+} cations, which cancels out the specific Zn−O distances.

TABLE 6: Number and Distances of Oxygen Nearest Neighbors in Zinc-Exchanged BEA Zeolites Determined from EXAFS Analysis

sample	Zn/Al	sample treatment	N_{Zn-O}[a]	r_{Zn-O} (Å)	$\Delta\sigma^2$ (Å^2)	E_0 (eV)
Zn/H-BEA	0.08	before	3.6	2.06	3.9×10^{-3}	−2.8
		activation	2.5	3.36	4.3×10^{-3}	4.1
Zn/H-BEA	0.08	after	4.3	1.96	1.7×10^{-2}	−3.6
		activation	1.8	3.00	3.9×10^{-2}	8.8
Zn/H-BEA	0.53	after	2.6	1.96	2.8×10^{-3}	−2.5
		activation	2.1	2.60	2.8×10^{-3}	8.1

[a] Number of nearest oxygen neighbors.

The analysis of the EXAFS using phase-shift and amplitude functions calculated by FEFF is summarized in Table 6. In dehydrated Zn/H-BEA (0.08 Zn/Al) four oxygen neighbors ($N_{Zn-O} = 4.3$) were found at a distance of 1.96 Å and somewhat less than two ($N_{Zn-O} = 1.8$) at 3.00 Å, while in the hydrated sample the number of neighbors in the first coordination sphere decreased and the bond length increased. Note that the number of oxygen neighbors in the second coordination sphere increased upon hydration in parallel to the Zn−O distances. This indicates strong interaction of zinc with framework oxygen in the dehydrated samples, which decreases upon hydration.

Conceptually, it is possible to exchange Zn^{2+} on six-, five-, and four-membered-ring positions in the BEA structure (denoted 6-MR, 5-MR, and 4-MR, respectively), which can be differentiated by the number and distance of the framework oxygen atoms surrounding the Zn^{2+} atoms. The local environment of Zn^{2+} atoms placed at the different ion exchange positions in zeolite Beta was calculated by quantum chemical cluster calculations and is compiled together with the relative energies (with respect to the energetically most stable position in the six-membered ring) in Table 7.

The energy of Zn^{2+} incorporation was lowest for the 6-MR position. For Zn^{2+} on the 5-MR position a slightly higher energy was calculated, while Zn^{2+} in the 4-MR position was significantly less favored in energy. This order of ion exchange sites was identical with that described for Zn^{2+} in Chabazite,[21] the relative energies, however, were lower, indicating that the BEA framework has a higher flexibility and, therefore, an ion exchange on structurally more constraint positions might also be possible.

The simulation of the local environment of Zn^{2+} at the three potential ion exchange positions resulted in a bimodal distribution of Zn−O distances below 2.2 Å and above 2.8 Å for the 6-MR and 5-MR positions, while Zn^{2+} on the 4-MR position is characterized by Zn−O distances below 2.2 Å. This clearly

TABLE 7: Local Environment and Relative Energy of Zn^{2+} at Potential Ion Exchange Positions

ion exchange position	distance to next neighbors r_{Zn-O} (Å)	N_{Zn-O} $r < 2.2$ Å	N_{Zn-O} $r > 2.8$ Å	ΔE (kJ/mol)
six-membered ring	1.90, 1.91, 1.97, 2.01, 3.43, 3.47	4	2	≡0
five-membered ring	1.98, 2.03, 2,12, 2.20, 2.83	4	1	9.7
four-membered ring	1.94, 1.97, 2.06, 2.07	4	0	33.8

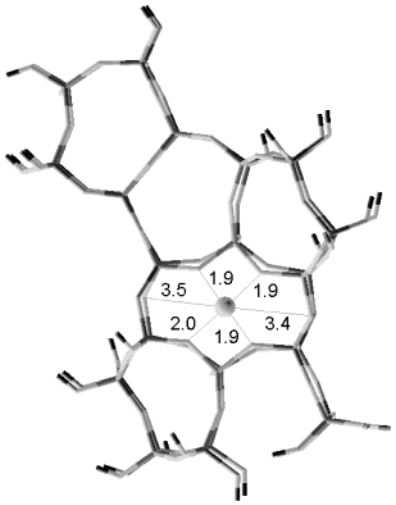

Figure 12. Preferred location of Zn^{2+} cations in zeolite BEA. Shown is zinc bound to the 6-MR position (distances in Å).

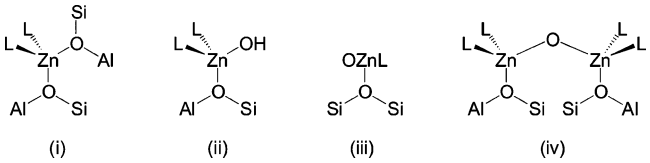

Figure 13. Possible Zn sites in Zn/H-BEA (L = framework oxygen or neutral ligand).

indicates that the majority of Zn^{2+} in Zn/H-BEA (0.08 Zn/Al) is located at the 6-MR positions (Figure 12), as the analysis of the EXAFS resulted in 4.3 oxygen neighbors at 1.96 Å and 1.8 oxygen neighbors at 3.0 Å. The slightly lower average coordination number for the oxygen atoms with distances above 2.8 Å could indicate that a minor part of the Zn^{2+} cations is located at 5-MR positions.

4. Discussion

4.1. Concentration of Acid Sites. Following the overall aluminum concentration measured by AAS, the maximum acid site concentration for the parent H-BEA is 1.36 mmol/g. Adsorption/desorption experiments with ammonia, however, led to a total acid site concentration of 0.46 mmol/g. This suggests that a significant fraction of the aluminum does not participate in the formation of acid sites. Note that the Brønsted acid site concentration for the parent H-BEA was even lower (0.14 mmol/g). Two types of Brønsted acid sites, isolated (3612 cm^{-1}) and hydrogen bonded (3750−3200 cm^{-1}), exist in H-BEA zeolite as concluded from IR spectroscopy. Basic probe molecules, such as CD_3CN, adsorb preferentially on the isolated Brønsted acid sites but hardly interact with Brønsted acid sites involved in hydrogen bonding. Quantification of IR spectra obtained after adsorption of pyridine and acetonitrile-d_3 showed that the concentration of Al^{3+} Lewis acid sites in dehydrated H-BEA was between 0.19 and 0.27 mmol/g. The discrepancies in the number of sites determined by using two different techniques clearly merits a more detailed discussion.

4.2. Nature and Formation of Lewis Acid Sites. The reversible and irreversible formation and the nature of aluminum Lewis acid sites in H-BEA is still under discussion. Brønsted acid sites, which are involved in hydrogen bonding interactions, were shown to have a higher tendency to dehydroxylate than isolated Brønsted acid sites.[32,37] The process is reversible as octahedrally coordinated Al^{3+} are able to reassume the tetrahedral lattice position.[41] Note that the reversibility of this process strongly suggests that the aluminum species remain close to their original position in the framework. Moreover, there are many literature suggestions that octahedrally coordinated aluminum is attached to the framework.[42] In H-Beta, octahedrally coordinated aluminum can be reverted to tetrahedrally coordinated aluminum during alkali ion exchange, treatment with a base, or simple heat treatment at temperatures above 100 °C.[43,44]

The observations of this study can be explained by a similar sequence of lattice modifications. In the partially hydrated H-BEA 16% of the total aluminum content (0.20 mmol/g) is associated with octahedral aluminum, 49% with well-defined tetrahedral aluminum (0.66 mmol/g), and 35% with "broad" tetrahedral aluminum (0.48 mmol/g). After activation and dehydration, 0.14 mmol/g isolated (tetrahedral) Brønsted acid sites were observed by IR spectroscopy of adsorbed acetonitrile-d_3. Dehydroxylation of adjacent Brønsted acid sites (which are involved in hydrogen bonding) leads to destruction of 0.54 mmol/g tetrahedral aluminum sites and only the resulting Al^{3+} Lewis acid sites (0.27 mmol/g) are available for adsorption of probe molecules. In this respect, it is known that dehydroxylation of two Brønsted acid sites leads to formation of one Al^{3+} Lewis acid site.[32,37,41] Assuming that neither the initially present "broad" tetrahedral nor the octahedral aluminum give rise to adsorption of probe molecules, the two methods provide exactly the same acid site concentration. Destruction of 82% of the initially present 0.66 mmol/g well-defined tetrahedral sites would provide a sample with 0.27 mmol/g of Al^{3+} Lewis acid and 12 mmol/g of Brønsted acid sites. The aluminum content not accounted for (0.68 mmol/g) is attributed to extraframework aluminum or amorphous silica−alumina, which give rise to aluminum species with a high quadrupolar coupling constant in ^{27}Al NMR.

The Lewis acidic Zn^{2+} cations may exist (i) ion exchanged to two tetrahedral aluminum sites (Zn/Al ≤ 0.50) requiring close neighborhood of the Al^{3+} sites, (ii) ion exchanged as $Zn(OH)^+$ involving one tetrahedral aluminum site (Zn/Al ≤ 1.00), or (iii) as neutral ZnO located at the pore wall or the outer surface (Zn/Al not limited) (Figure 13). Note that the formation of $Zn(OH)^+$ species has been reported only for hydrated zeolites.[22] Recently, Iglesia et al. showed by X-ray adsorption spectroscopy on zinc-exchanged ZSM-5 that $Zn(OH)^+$ species are not stable and dehydrate upon thermal treatment.[4]

In the presence of another nearby SiOHAl group $Zn(OH)^+$ might eliminate water and form directly or indirectly a bridge between two SiO^-Al sites. In this context, van Santen et al. concluded from DFT studies that Zn^{2+} cations in dehydrated chabazite are best stabilized on positions where at least two tetrahedral aluminum atoms are in the vicinity.[21] Thus, we infer that pairs of tetrahedral framework aluminum atoms,[45] which are sufficiently close to allow the bridging Zn^{2+} cation to balance

the lattice charge, are the preferential ion exchange positions for zinc. If the framework aluminum atoms are further apart (max 1.2 nm), two Zn^{2+} cations on SiO^-Al sites are bridged by an oxygen atom (iv).

In the presently investigated BEA both isolated and vicinal aluminum tetrahedra exist as evidenced by the bands attributed to isolated and clustered SiOHAl bands. With increasing degree of Zn^{2+} cation exchange the concentration of isolated Brønsted acid sites decreased initially from 0.14 to 0.10 mmol/g relative to the parent H-BEA (as determined from the IR spectra of adsorbed acetonitrile-d_3 and pyridine and by TPD of ammonia and 2-propylamine). Above a Zn^{2+} concentration of approximately 0.02 Zn/Al the concentration of isolated OH remained approximately constant. This indicates that the protons of isolated Brønsted acid sites cannot be exchanged in a stable manner by Zn^{2+} cations. The minor initial decrease is caused by destruction of some Brønsted acid sites upon zinc exchange and subsequent calcination.

The broad IR absorption band (3750−3200 cm^{-1}) remained unchanged after sorption of basic probe molecules such as NH_3, CD_3CN, or pyridine. This indicates that these OH groups have no significant acidity and, therefore, the protons cannot be exchanged by zinc cations. Furthermore, after zinc exchange no significant changes in the intensity of this absorption band were observed. Nevertheless, the quantification appeared to be difficult as H-bonding interactions lead to broadening and increasing intensity of this IR band.[34]

The concentration of Al^{3+} Lewis acid sites decreased linearly (0.22−0 mmol/g) with increasing Zn^{2+} content as deduced from the IR spectra of adsorbed acetonitrile-d_3. In parallel, the concentration of Zn^{2+} Lewis acid sites increased linearly. This indicates a direct correlation between Zn^{2+} incorporation and decrease in Al^{3+} Lewis site concentration. We conclude, therefore, that Zn^{2+} ion exchange occurs preferentially on neighboring aluminum pairs. By means of the Zn^{2+} exchange, neighboring tetrahedral framework aluminum pairs are stabilized. Remaining pairs of Brønsted acid sites are quantitatively dehydroxylated during the activation procedure. Note that the isolated SiOHAl are stable, but it is impossible to stabilize $Zn(OH)^+$ groups.

The constancy of the total number of Lewis acid sites (Zn^{2+} and Al^{3+} Lewis acid sites) in the range $0 \leq Zn/Al \leq 0.26$ as seen by IR spectroscopy of adsorbed pyridine (450 °C) shows that one Zn^{2+} cation formally replaces one Al^{3+} Lewis site. These results are in agreement with those reported by Wichterlová et al. for incorporation of Co^{2+} in BEA zeolites (0−0.25 Co/Al), suggesting similar characteristics for the two cations.[32]

The presence of the two different Zn^{2+} ion exchange sites is also manifested by the decomposition of 2-propylamine (propene desorption peaks). The high-temperature peak (476 °C) increased in intensity linearly with the zinc loading from 0 to 0.15 Zn/Al (Zn^{2+} incorporated on vicinal aluminum). The second zinc site (corresponding to the desorption maximum at 394 °C) is present in this range of zinc loading only in small concentrations. However, its concentration increased markedly between 0.15 and 0.26 Zn/Al. In this concentration range pairs of Zn^{2+} cations with a bridging oxygen are formed that balance the charge of SiO^-Al sites, which are not further apart than 1.2 nm (Figure 13, iv). It is interesting to note that even the small variations in the acidity of these sites leads to the clear differentiation of their chemical reactivity.

The most stable ion exchange positions for Zn^{2+} cations were identified by X-ray absorption spectroscopy. For Zn/H-BEA (0.08 Zn/Al) four Zn−O distances of around 2.0 Å and two of around 3.0 Å were observed. Quantum chemical cluster calculations revealed that this is a clear indication for the location of Zn^{2+} at six-membered oxygen ring positions. In addition, this position was found to be the energetically most stable ion exchange position for Zn^{2+} within the BEA structure.

In the sample with 0.26 Zn/Al all aluminum pairs are coordinated with Zn^{2+} cations. As has been discussed the stability of $Zn(OH)^+$ on isolated SiO^-Al sites is so low that these cations do not withstand thermal treatment. It is speculated that the ion- exchanged sites disproportionate into SiOHAl groups and ZnO nanocrystals that eventually migrate out of the BEA pores.

This phase is indirectly evidenced by the adsorption of pyridine and acetonitrile, but its nature could not be characterized by an averaging technique such as X-ray absorption spectroscopy. At high zinc loading (0.53 Zn/Al) this phase will amount to approximately 60% of the total Zn^{2+} in the sample. The lower Lewis acid strength of Zn^{2+} in this phase is reflected in the low thermal stability of, e.g., the acetonitrile adsorption complex. The corresponding TPD peak occurred already at 176 °C compared to 359 and 456 °C for acetonitrile desorbing from Zn^{2+} at exchange positions. The low reactivity of the phase was also seen in activity for hydroamination catalyzed by Zn/H-BEA. The catalytic activity increased linearly with the zinc content up to 0.26 Zn/Al, while it remained constant at higher concentrations.[6] It should be emphasized that ZnO is generally inactive to catalyze hydroamination reactions.

5. Conclusions

The present results indicate that it is possible to prepare well-defined Zn^{2+} ion exchanged zeolites BEA. Materials with Zn^{2+} bridging the oxygens of two vicinal aluminum tetrahedra and $(Zn-O-Zn)^{2+}$ species bridging two tetrahedra being somewhat further apart can be prepared in high yield. The combination of EXAFS and structure simulation indicate that the zinc cations are located preferentially in six-membered oxygen rings most likely those facing the main channel system. These materials contain, however, always a fraction of Brønsted acid sites, because Zn^{2+} or $Zn(OH)^+$ cannot be stabilized at isolated Brønsted acid sites. Attempts to exchange these sites selectively with monovalent cations are under way.

The strongly electronegative environment of the zeolite enhances the Lewis acid strength far beyond that of Zn^{2+} in bulk or nanocrystalline ZnO. On the basis of the thermal stability of adsorbed bases, the strength of the Lewis acid site is comparable to that of accessible Al^{3+} cations. This strong Lewis acidity together with the open structure of zeolite BEA makes these materials a group of highly active catalysts for Lewis acid or Brønsted/Lewis acid-catalyzed reactions. It should be emphasized that the high self-organization of Zn^{2+} in zeolite ion exchange sites could potentially lead to a new class of well-defined heterogeneous catalysts for fine chemical synthesis.

Acknowledgment. The financial support from DSM and Dr.-Ing. Leonhard-Lorenz-Stiftung is gratefully acknowledged. The XAFS experiment were carried out at HASYLAB, DESY, Hamburg, Germany, and supported by the TMR-Contract ERBFMGECT950059 of the European Community. Xaver Hecht and Martin Neukamm are thanked for their experimental support.

References and Notes

(1) Haw, J. F.; Nicholas, J. N.; Song, W.; Deng, F.; Wang, Z.; Xu, T.; Heneghan, C. S. *J. Am. Chem. Soc.* **2000**, *122*, 4763.

(2) Maxwell, I. E.; Stork W. H. J. In *Studies in Surface Science and Catalysis*; van Bekkum, H., Flanigen, E. M., Jansen, J. C., Eds.; Elsevier: Amsterdam, The Netherlands, 1991; Vol. 58, p 571.

(3) Djakovitch, L.; Koehler, K. *J. Am. Chem. Soc.* **2000**, *132*, 5990.

(4) Biscardi, J. A.; Meitzner, G. D.; Iglesia E. *J. Catal.* **1998**, *179*, 192.

(5) Ono, Y. *Catal. Rev. Sci. Eng.* **1992**, *34*, 179.

(6) Penzien, J.; Müller, T. E.; Lercher, J. A. *Microporus Mesoporous Mater.* **2001**, *48*, 285.

(7) Penzien, J.; Müller, T. E.; Lercher, J. A. *J. Chem. Soc., Chem. Commun.* **2000**, *18*, 1753.

(8) Müller, T. E. In *Encyclopedia of Catalysis*; Horváth, I. T., Ed.; John Wiley & Sons: New York, 2002.

(9) Hagen, A.; Roessner, F. In *Studies in Surface Science and Catalysis*; Krager, H. G., Weitkamp, J., Eds.; Elsevier: Amsterdam, The Netherlands, 1999; Vol. 98, p 189.

(10) Onyesták, G. Y.; Kalló, D. In *Studies in Surface Science and Catalysis*; Delmon, B., Froment, G. F., Eds.; Elsevier: Amsterdam, The Netherlands, 1987; Vol. 34, p 605.

(11) Onyesták, G. Y.; Papp, J.; Kalló, D. In *Studies in Surface Science and Catalysis*; Karge, H. G., Weitkamp, J., Eds.; Elsevier: Amsterdam, The Netherlands, 1989; Vol. 46, p 241.

(12) Senger, S.; Radom, L. *J. Am. Chem. Soc.* **2000**, *122*, 2613.

(13) Jansen, J. C.; Creyghton, E. J.; Njo, S. L.; van Koningsveld, H.; van Bekkum, H. *Catal. Today* **1997**, *38*, 205.

(14) Pandey, P. A.; Singh, A. P. *Catal. Lett.* **1997**, *44*, 129.

(15) Ma, Y.; Wang, Q. L.; Jiang, W.; Zuo, B. *Appl. Catal. A* **1997**, *165*, 199.

(16) Treacy, M. M. J.; Newsam, J. M. *Nature* **1988**, *332*, 249.

(17) Higgins, J. B.; LaPierre, R. B.; Schlenker, J. L.; Rohrmann, A. C.; Wood, J. D.; Kerr, G. T.; Rohrburg, G. J. *Zeolites* **1986**, *8*, 446.

(18) Ressler, T. *J. Synchrotron Radeat.* **1998**, *5*, 118.

(19) Ankudinov, A. L.; Ravel, B.; Rehr, J. J.; Conradson, S. D. *Phys. Rev. B* **2000**, *62*, 2437.

(20) Delley, B. *J. Chem. Phys.* **1990**, *92*, 508.

(21) Barbosa, L. A. M. M.; van Santen, R. A. *J. Am. Chem. Soc.* **2001**, *123*, 4530.

(22) Barbosa, L. A. M. M.; van Santen, R. A. *Catal. Lett.* **1999**, *63*, 97.

(23) Gorte, R. J. *Catal. Lett.* **1999**, *62*, 1.

(24) Eubanks, J. R. I.; Sims, L. B.; Fry, A. *J. Am. Chem. Soc.* **1991**, *113*, 8821.

(25) Bourns, A. N.; Frosst, A. C. *Can. J. Chem.* **1970**, *48*, 133.

(26) Kirby, A. J.; Logan, C. L. *J. Chem. Soc., Perkin Trans. 2* **1978**, 642.

(27) Penzien, J.; Haessner, C.; Jentys, A.; Köhler, K.; Müller, T. E.; Lercher, J. A. *J. Catal.* In press.

(28) Kirisci I.; Flego, C.; Pazzuconi, G.; Parker, W. O., Jr.; Millini, R.; Perego, C.; Bellussi G. *J. Phys. Chem.* **1994**, *98*, 4627.

(29) Bourgeat-Lami, E.; Massiani, P.; Di Renzo, F.; Espiau, P.; Fajula, F. *Appl. Catal.* **1991**, *72*, 139.

(30) Stockenhuber, M.; Lercher, J. A. *Microporous Mater.* **1995**, *3*, 457.

(31) Steiner, T. *Angew. Chem.* **2002**, *114*, 50.

(32) Bortnosvsky, O.; Sobalík, Z.; Wichterlová, B. *Microporous Mesoporous Mater*. **2001**, *46*, 265.

(33) Jähnchen, J.; Peeters, M. P. J.; van Wolput, J. H. M. C.; Wolthuizen, J. P.; Lohse, U.; van Hoof, J. H. C. *J. Chem. Soc., Faraday Trans.* **1994**, *90* (7), 1033.

(34) Desiraju, G. R.; Steiner, T. *The Weak Hydrogen Bond*; Oxford Science Publication: New York, 1999; p 51.

(35) Palmenschikov, A. G.; van Santen, R. A.; Jänchen, J.; Meijer, E. *J. Phys. Chem.* **1993**, *97*, 11071.

(36) Wichterlová, B.; Tvarková, Z.; Sobalík, Z.; Sarv, P. *Microporous Mesoporous Mater.* **1998**, *24*, 223.

(37) Borade, R. B.; Clearfield, A. *J. Phys. Chem.* **1992**, *96*, 6729.

(38) See also: Beers, A. E. W.; van Bokhoven, J. A.; Kapteijn, F.; Moulijn, J. *J. Catal.* **2003**, *218*, 239.

(39) Kunzl, V. *Collect. Czech. Chem. Commun.* **1932**, *4*, 213.

(40) Groothaert, M. H.; van Bokhoven, J. A.; Battiston, A. A.; Weckhuysen, B. M.; Schoonheydt, R. A. *J. Am. Chem. Soc.* **2003**, *125*, 7629.

(41) Kuehl, G. H.; Timken, H. K. C. *Microporous Mesoporous Mater.* **2000**, *35*−*36*, 521.

(42) Bourgeat-Lami, E.; Massiani, P.; Di Renzo, F.; Espiau, P.; Fajula, F.; Des Courières, T. *Appl. Catal.* **1991**, *72*, 139.

(43) van Bokhoven, J. A.; van der Eerden, A. M. J.; Koningsberger, D. C. *Stud. Surf. Sci. Catal*. **2002**, *142*, 1885.

(44) van Bokhoven, J. A.; van der Eerden, A. M. J.; Koningsberger, D. C. *J. Am. Chem. Soc.* **2003**, *125*, 7435.

(45) Van Santen, R. A.; Kramer, G. J. *Chem. Rev.* **1995**, *95*, 637.